Temperature dependent lattice misfit and coherency of Al_3X (X = Sc, Zr, Ti and Nb) particles in an Al matrix

Saumitra Saha, T. Z. Todorova, J. W. Zwanziger*

Department of Chemistry, Dalhousie University, PO Box 15000, Halifax, NS, Canada B3H 4R2

Abstract

The lattice coherency and critical radii for Al_3X precipitates in an aluminum matrix were computed using first-principles methods. From density functional perturbation theory and the quasi-harmonic approximation, the unit cell parameters as a function of temperature were determined for Al_3Sc, Al_3Zr, Al_3Ti, and Al_3Nb in the $L1_2$ structure, and for Al_3Ti and Al_3Nb in their more stable DO_{22} structures. From these data the lattice misfit and critical radii were determined. It was found that Al_3Sc and Al_3Zr behave similarly, with increasing critical radii and decreasing misfit as a function of temperature, while Al_3Ti and Al_3Nb behaved oppositely. Furthermore, the DO_{22} phases showed uniformly poor lattice coherence and very small critical radii. Superior alloy properties in Al/Al_3X systems are suggested to require stabilization of the $L1_2$ phase in the precipitated particles.

1. Introduction

Aluminum matrix composites are an important class of material for application in microelectronic, automotive and aerospace industries. These lightweight but strong materials offer good mechanical and elastic properties as well as cast-ability and thermal stability. The trialuminide compounds with early transition metals (Sc, Ti, Zr, V, Hf) are usually used as reinforcement. Aluminum alloys reinforced with trialuminide particles (Al_3Sc, Al_3Zr, Al_3Ti, Al_3Nb *etc*.) are of interest because of their high specific strength, high specific modulus, and excellent properties both at ambient and elevated temperature [1–6]. Of particular interest is the possible use as of these trialuminides as precipitates for high-temperature, creep-resistant Al-based alloys. These trialuminide compounds have attractive properties such as high melting points, low mass densities,and good oxidation resistances [7].

There is a specific interest in Al-Sc alloys as high strength material because adding Sc significantly increases the strength and stiffness of the alloy compared to pure Al [8, 9]. The effect of Sc on the properties of Al-Sc alloys include 20–50% increase in mechanical strength and significant grain refinement compared with other high strength Al alloys. These alloys also show reduced surface re-crystallization improved weld strength, reduced hot-cracking as well as increased plasticity [10], durability and formability [11]. To a significant extent, Al_3Sc precipitates in the solid Al matrix homogeneously. The precipitates are coherent with the Al matrix and normally have a spherical appearance.

Encouraged by the strengthening and other properties of Al_3Sc precipitate, there is a growing interest in the properties and effect of other similar particles such as Al_3Zr, Al_3Ti, and Al_3Nb. The interest in Al_3Ti and Al_3Zr are due to their higher melting point ($\sim$ 1623 K) and relatively low density (3.4 g cm^{-3}) [1]. Furthermore, Zr and Ti have low diffusivity and solubility in aluminum [12, 13]. As a result, Al_3Zr and Al_3Ti can be expected to exhibit a low coarsening rate at elevated temperature [13]. Interest in Al_3Nb is due to the considerable strength and

*Corresponding author
Email address: jzwanzig@dal.ca (J. W. Zwanziger)

hardness it imparts [14, 15]. Despite the brittleness of Al_3Nb at ambient and moderate temperature, no cracks are observed, due to the presence of the thin interdendritic film of ductile α-Al solid solution, which accommodates stresses and prevents crack propagation. Addition of Sc and Zr to Al also demonstrate potential for developing creep-resistant, thermally stable alloys at elevated temperatures [12].

During the aging process nanometer scale trialuminide precipitates are formed from the supersaturated Al-Sc, Al-Zr and Al-Ti and Al-Nb solid solutions. These trialuminide precipitates have the $L1_2$ crystal structure. Compared to Nb, Zr and Ti, Sc has higher diffusivity in an Al matrix and the composite materials are only resistant to coarsening up to $\sim$ 300 °C [12, 16, 17]. Although Nb, Zr and Ti have lower diffusivity in an Al matrix, the $L1_2$ structures of Al_3Zr and Al_3Ti are thermodynamically metastable [12, 13, 18]. Al_3Ti and Al_3Nb are both stable in the the DO_{22} structure, which is less desirable than the $L1_2$ structure from the point of view of brittleness. At room temperature the $L1_2$ precipitate particles show coherency with the Al matrix. The parameter that reflects the coherency is the lattice parameter.

However, the lattice thermal expansion of the precipitate particles are different from that of the Al matrix. Moreover, the lattice thermal expansion of the precipitate particles depends on the temperature differently and thus makes the misfit temperature-dependent. There are some experimental data on the lattice misfit of Al_3Sc and Al_3Nb and analysis of its temperature dependency. However, no experimental data and analysis are available for Al_3Zr and Al_3Ti. Here, we applied first-principles methods to calculate the thermodynamic data for all these precipitates as well as bulk Al, including detailed investigation of the $L1_2$ structures and the DO_{22} structures for the Al_3Nb and Al_3Ti compounds, where this structure is more stable. We also discuss the predicted lattice coherency as a function of temperature.

2. Methods

We calculated the volumetric coefficient of thermal expansion, $\alpha_V = (\partial \ln V/\partial T)$, of Al_3X within the quasi-harmonic approximation (QHA). This approach permits the estimation of temperature-dependent effects through a combination of calculations at zero Kelvin but varying volume, and fitting to a reasonable equation of state. Typical density-functional theory (DFT) calculations model the system implicitly at zero Kelvin, and subsequent linear response calculations of atomic perturbations yield the phonon frequencies strictly in the harmonic approximation. The resulting harmonic model of a solid cannot predict the thermal expansion coefficient, the thermal dependence of the elastic properties, or a number of other features.

In the QHA, phonon modes and frequencies are computed at a range of unit cell volumes around the zero temperature relaxed value. Then, from these calculations the free energy is constructed as a function of both temperature and cell volume, using the standard expression

$$F(V,T) = U_0(V) + \frac{1}{2}\sum_{\mathbf{q},\nu} \hbar\omega\left(\mathbf{q},\nu \mid V\right) + k_B T \sum_{\mathbf{q},\nu} \log\left(1 - \exp\left(\frac{-\hbar\omega\left(\mathbf{q},\nu \mid V\right)}{k_B T}\right)\right). \quad (1)$$

Here $\omega\left(\mathbf{q},\nu \mid V\right)$ is the frequency of phonon ν at wavevector $\mathbf{q}$ and cell volume V, and U_0 is the cell energy as computed at zero temperature. Thus the need to compute true finite-temperature effects of the phonons is avoided, but their effect on volume is included parametrically in the free energy. Finally, at each temperature the free energy as a function of volume is fit to an equation of state (for example the Murnaghan equation), in the cubic case, or at least parameterized, in the more general case, to extract the temperature-dependent cell volume. This volume may be differentiated as a function of temperature to obtain the thermal expansion coefficient.

The DFT calculations were carried out using the Abinit software package, a common project of the Université Catholique de Louvain, Corning Incorporated, and other contributors (URL http://www.abinit.org). This code package provides an implementation of DFT for periodic systems using a planewave basis and pseudopotentials [19, 20]. Phonons are calculated within the context of density functional perturbation theory [21, 22], and thermal properties (specifically the vibrational contribution to the free energy) through a subsequent integration over the phonon degrees of freedom [23].

Norm-conserving pseudopotentials of optimized Vanderbilt type were used [24], together with the Perdew-Burke-Ernzerhof exchange and correlation function-

als [25]. A planewave energy cutoff of 25 Ha together with a k-point spacing of 0.04 $Å^{-1}$ were used, the latter generated by a shifted 6×6×6 Monkhorst-Pack grid; these values were sufficient to converge the cell stress to better than 0.1%. The metallic occupancy of the levels was implemented using the cold-smearing method to mitigate the effect of the changing band occupation with k-point on the minimization procedure used to solve the DFT equations [26]. The smearing procedure itself is non-physical but leads to better stability in solfing the DFT equations, and the smearing parameter used can be treated as a convergence parameter. We used 0.03 Ha, which was determined by minimizing the total energy at the experimental cell volume of aluminum, and then used for the other compounds as well. The phonons were computed by the linear response component of ABINIT, using the same reciprocal space grid to generate the **q** points, at a range of cell volumes generated by varying the lattice parameters from −2.5% to +2.5% around the relaxed value, in steps of 0.5%. For the cubic $L1_2$ structures this variation amounts to a dilation of the unit cell and required 11 separate phonon dispersion calculations, while for the tetragonal DO_{22} phases both the *a* and *c* cell lengths were varied, leading to 121 phonon dispersion calculations. The phonon free energies were then computed in 1 deg intervals at each volume, by interpolating the phonon frequencies onto increasingly dense grids until convergence. Finally, the total free energy (cell energy plus vibrational free energy) was fit as a function of volume to the Murnaghan equation of state, in the cubic case, and to a two-dimensional spline, in the tetragonal case, to obtain the optimal cell volume at each temperature. The coefficient of thermal expansion was obtained by numerical differentiation of the volume versus temperature data using a four-point formula, in the cubic case; the tetragonal cases lead to somewhat noisier data and so a fourth-order polynomial fit to the $V(T)$ data was determined and then differentiated analytically.

3. Results

Calculated lattice constants, corrected to room temperature (298 K) using the procedures outlined above, are presented in Table 1 and compared to experiment and other calculations where available. The lattice parameters calculated this work agree well with the experimental

Table 1: Computed lattice parameters for the compounds studied here, and comparison where possible to experiment and other calculations. Our calculations have been corrected to room temperature (298 K) using the Quasi-Harmonic Approximation.

Compound	Method	Lattice parameter (Å)
Al	(this work)	4.069
	Expt (RT) [27]	4.049750
Al_3Nb, $L1_2$	(this work)	4.019
DO_{22} (a)		3.854
(c)		8.706
(a)	Expt (RT) [28]	3.801
(c)		8.538
Al_3Sc	(this work)	4.125
	Expt (RT) [29]	4.103(1)
Al_3Ti, $L1_2$	(this work)	3.998
	Expt (RT) [30]	3.967
DO_{22} (a)	(this work)	3.868
(c)		8.628
(a)	Expt (RT) [31]	3.8537(3)
(c)		8.5839(13)
Al_3Zr	(this work)	4.122
	Expt (RT) [30]	4.08

Table 2: Formation energies in kJ/mol of various phases studied here, relative to their constituents.

Al_3Sc ($L1_2$)	-182.7
Al_3Zr ($L1_2$)	-191.6
Al_3Nb ($L1_2$)	-113.8
(DO_{22})	-170.2
Al_3Ti ($L1_2$)	-157.6
(DO_{22})	-160.4

and other simulation data, showing the typical slight dilation (about 0.5%) due to the use of the PBE exchange and correlation functional. In the $L1_2$ structure, all listed have a similarly small lattice misfit with Al and could be considered coherent with the Al lattice. The DO_{22} structures are clearly farther from coherent fit with Al.

The stabilities of the various phases relative to their components are shown in Table 2. These values represent the formation energy for the chemical reaction $3Al + X \rightarrow Al_3X$, and were obtained from the total energy from the DFT calculation for each phase in its ground state (low temperature) together with the energies for the pure elements also obtained from DFT using the methods outlined above. These results show that all compounds studied here are stable relative to their constituents, but that the DO_{22} phases are stable relative to the $L1_2$ phases, when they exist. Additionally, while the Al_3Ti DO_{22} phase is slightly stable relative to $L1_2$, in Al_3Nb the DO_{22} stability is quite substantial.

Fig. 1 shows the coefficient of volume thermal expansion α_V of aluminum, and Fig. 2 shows the computed α_V for the trialuminides studied here. Our first principle results for α_V of Al shows a very good agreement with the experimental measurement of temperature-dependent α_V of Al [32, 33].

Our results for Al_3Sc agree well with the result from previous first principle simulation [34] and experimental measurement [35]. At 298 K ref. [34] reports a value of 14.5×10^{-6} K^{-1} for the coefficient of linear thermal expansion α_L, while we obtain 14.3×10^{-6} K^{-1}. Note that Fig. 2 shows the coefficient of volume thermal expansion α_V, while for cubic $L1_2$ structures $\alpha_V = 3\alpha_L$. Both results from the first principles calculations slightly underestimate the experimental value of $(16\pm1)\times10^{-6}$ K^{-1} [35].

Experimental thermal expansion data for trialuminide

Figure 1: Computed coefficient of volume thermal expansion α_V for aluminum (solid line) together with experimental data [32, 33].

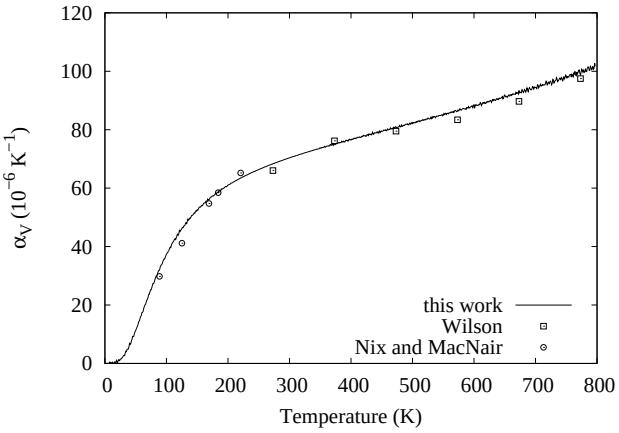

Figure 2: Computed coefficient of volume thermal expansion α_V for Al_3X ($L1_2$ structures: Al_3Nb red, Al_3Sc black, Al_3Ti blue, and Al_3Zr green; DO_{22} structures: Al_3Nb orange, Al_3Ti purple, color on-line).

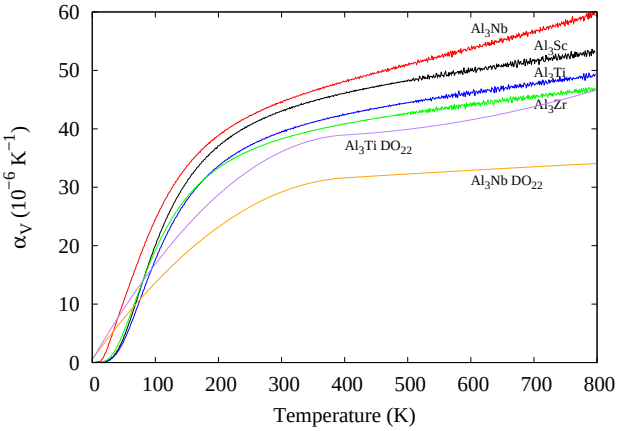

intermetallics are limited [35]. We have not found reliable thermal expansion data for Al_3Zr in literature. Our comparison of the coefficient of thermal expansion of Al_3Zr and Al_3Sc, presented in Fig. 2, shows that Al_3Zr has lower coefficient of thermal expansion than that of Al_3Sc. The differences in coefficient of thermal expansion increases minimally with increasing temperature. There is no significant difference in the coefficients of thermal expansion of Al_3Zr and Al_3Ti in the $L1_2$ structure. Our calculated thermal expansion coefficient of Al_3Zr and Al_3Ti are comparable with the measurement for ternary $Al_3(Sc_{0.75},Zr_{0.25})$ and $Al_3(Sc_{0.75},Ti_{0.25})$ intermetallic phases [35]. In the DO_{22} structure, Al_3Nb has been reported to have a coefficient of linear thermal expansion of 9.6×10^{-6} K^{-1} at room temperature [36], which is similar to our value ($9.6 \times 3 = 28.8$ compared to 29.1). For DO_{22} Al_3Ti, an FP-LAPW calculation yielded about 46×10^{-6} K^{-1}, to be compared with our value of 36.0×10^{-6} K^{-1} [37]

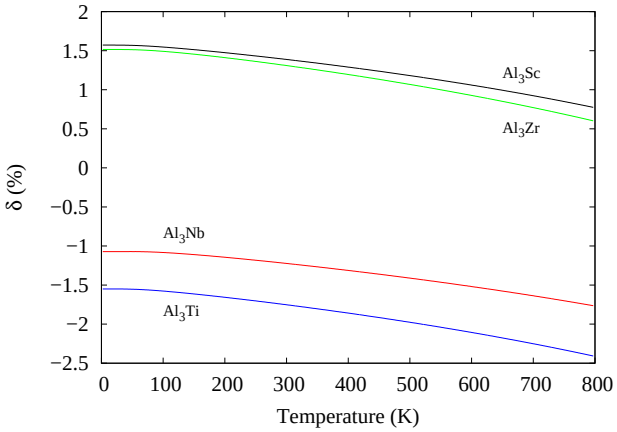

Figure 3: Lattice misfit of $L1_2$ Al_3X relative to aluminum, as a function of temperature (Al_3Nb red, Al_3Sc black, Al_3Ti blue, and Al_3Zr green, color on-line).

4. Discussion

4.1. Lattice misfit of Al_3X in the Al matrix

From the data computed in the QHA for the temperature-dependent cell volume, the temperature-dependent lattice misfit δ between the Al matrix and precipitate can be calculated as

$$\delta = \frac{a_{Al_3X} - a_{Al}}{a_{Al}} \qquad (2)$$

where a is the lattice constant of the indicated species in the $L1_2$ phases, and either the a or $c/2$ lattice constants for the DO_{22} phases.

In formulating the lattice mismatch, here we considered the lattice parameter changes due to thermal expansions only. We also assumed perfect crystal structures of both the Al matrix and trialuminide precipitates. However, there are other factors that influence the change in lattice parameters. These factors have more influence on the Al matrix than on the precipitates as the volume ratio of the matrix is significantly higher. The two factors that have significant contributions on lattice parameter are the vacancies and the transition metal impurities in solid solutions.

With increasing temperature the equilibrium vacancy concentration increases. Likewise, increasing number of impurities are introduced into the solid solution with increasing temperature. The temperature dependent concentrations of vacancies and impurities can be estimated from their formation enthalpy and entropy. Røyset and Ryum [38] analyzed the effect of vacancies and impurities on the lattice misfit in the Al/Al_3Sc system. They used available data from literature to estimate the concentration of vacancies in Al matrix and impurities in solid solution. Their analysis shows that the vacancies and impurities have influences on lattice misfit with approximately the same magnitude, but with opposite direction [38]. As a result, the net effect of these two factors are negligible. Assuming that Zr, Ti, and Nb have similar effects as Sc, we therefore, did not consider these factors in our analysis and calculated the temperature dependent lattice misfit applying the formula in Eq. 2.

Fig. 3 shows the temperature-dependent lattice misfit of Al_3X for the $L1_2$ structures, and Fig. 4 shows the same information for the DO_{22} structures. The temperature dependence of lattice misfit of Al_3Sc with Al matrix calculated in this study from first principles methods agrees very well with the data presented in ref. [38]. There is no experimental or theoretical data available for the temperature dependence of lattice misfit for the other compounds.

The comparison of changes in lattice misfits with temperature for presented in Fig. 3 show different trends for Al_3Ti and Al_3Nb compared with Al_3Sc and Al_3Zr. With

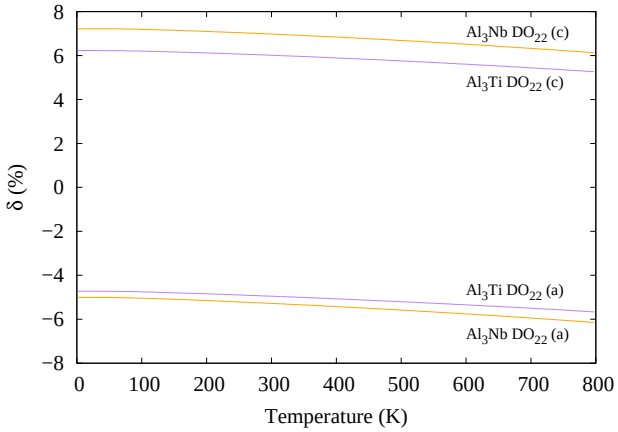

Figure 4: Lattice misfit of DO_{22} Al_3X relative to aluminum, as a function of temperature (Al_3Nb purple, Al_3Ti orange, color on-line).

temperature the lattice mismatch of both Al_3Ti and Al_3Nb increases. At room temperature the lattice parameters of Al_3Nb and Al_3Ti are about 1.5% smaller than that of Al matrix. However, the thermal expansion of the Al matrix is higher than the thermal expansion of Al_3Nb and Al_3Ti at all temperatures. Moreover, the difference in thermal expansion grows with temperature (Fig. 2). Thus, the higher thermal expansion of Al and smaller initial lattice parameter of Al_3Nb and Al_3Ti leads to an increase in misfit with temperature.

No experimental or theoretical data on temperature dependence of the lattice mismatch between pure Al_3Ti or Al_3Nb and Al was found. Harada and Dunand [35] calculated the lattice mismatch between $Al_3(Sc_{0.75}Ti_{0.25})$ and Al from the measured average coefficient of thermal expansion. Their results predicted a significant reduction of mismatch with the addition of Ti in the Sc sublattice. This result can be explained by the lower Shannon radius of Ti compared to Sc combined with Vegards law. Replacement of Sc with Ti, therefore, contributes in lowering the lattice parameter of Al_3Sc. However, the room temperature lattice parameter of structures with a dominant proportion of Sc in the X sublattice of Al_3X is still higher than that of the Al matrix. For pure Al_3Ti structure or the structure with Ti dominated X sublattice, the equilibrium lattice parameter is lower than that of Al. This result suggests an optimal range of Ti on the X sublattice of between 25% to 50%, which could significantly improve the lattice coherency of $Al_3(Sc,Ti)$. Harada and Dunand [39] experimentally measured the maximum solubility of X in ternary $L1_2$-$Al_3(Sc,X)$ intermetallics phases and their lattice parameter. Their measurement shows that the lattice mismatch of $Al_3(Sc,Ti)$ with Al at maximum solubility of 41% reduces the lattice mismatch from 1.33% to 0.32% at room temperature [15, 39]. Further studies are needed to define the temperature dependency of the lattice mismatch and find the optimal concentration of Ti in $Al_3(Sc,Ti)$ with the best lattice coherency at elevated temperature.

In contrast to the Al_3Nb and Al_3Ti cases, the lattice misfit of Al_3Sc and Al_3Zr with Al matrix decrease with temperature. The initial lattice parameters of Al_3Sc and Al_3Zr are higher than the lattice parameter of Al, so the higher thermal expansion of Al leads to closing the gap between the lattice parameter of Al and Al_3Sc and Al_3Zr. Addition of Zr in ternary $L1_2$-$Al_3(Sc,Zr)$ intermetallics phases also contribute in reduction of lattice mismatch. At the maximum solubility of 51% for Zr in $Al_3(Sc,Zr)$ reduces the lattice mismatch from 1.33% to 1.12% at room temperature. Our results for the temperature dependence of lattice misfit agree well with the calculation of ref. [35, 38]. Both calculations are based on the same average coefficient of thermal expansion measured in Ref. [35].

The lattice mismatches of the DO_{22} phases are considerably worse than the $L1_2$ structures considered above. As compared to the cubic $L1_2$ structure, the DO_{22} body-centered tetragonal structure includes a base with a parameter decreased from cubic, while the c parameter is elongated from the ideal $2 \times a$ for coherency. Fig. 4 shows that the a parameters are some 5% too short for coherence with the Al matrix, while the $c/2$ value (the fit of a cube carved out of the tetragon) is about 6% too long. Clearly the DO_{22} phases, which are somewhat stable for Al_3Ti and very stable for Al_3Nb (see Table 2), must be avoided in order to develop a composite with good precipitate matrix coherency.

4.2. Critical diameter and loss of coherency

During the precipitation and aging process particle coherency plays an important role in the coarsening behavior. At some stage of the aging process, the precipitation rate decreases and precipitated particles start to grow. These processes are temperature-dependent [40].

The particle growth will increase the matrix strain and inevitably lead to a critical size. Beyond this critical size, it is energetically more favorable to introduce an interfacial dislocation at the matrix/precipitate interface than to increase further the matrix strain. At this critical radius, particles begin to lose coherency and the coarsening process begins. This scenario has been observed with Al_3Sc [41].

The critical size of a precipitate particle can be modeled simply from the lattice parameters. According to this simple model, at the critical diameter, the misfit over the whole particle diameter is equal to the Burgers vector of the Al matrix [38]. However, a complete model for coherent precipitates must include the elastic interactions. The lattice mismatch between the precipitate and matrix phases increases the elastic interaction that determines precipitate shape and alignment [42, 43]. The elastic interaction is the driving force for the formation of the interfacial dislocations. As the total energy of the matrix with precipitates is conserved, the increase of interfacial energy by the introduction of dislocations is compensated by the decrease of elastic energy due to the relaxation of lattice distortion. The balance between the increase in interfacial energy and relaxation in elastic energy at the critical diameter for coherent/semicoherent transition has been derived as [40, 44]:

$$\pi d_{\mathrm{crit}}^2 \sigma_{\mathrm{dis}} = \pi d_{\mathrm{crit}}^3 G\delta^2 \frac{(1+\nu)}{3(1-\nu)} \tag{3}$$

where σ_{dis} is the energy of interfacial dislocation network per unit area, δ is the lattice misfit between the precipitate and the matrix, and G and ν are shear modulus and Poisson ratio of the matrix, respectively. The energy of the dislocation network σ_{dis} is expressed as [44]:

$$\sigma_{\mathrm{dis}} = \frac{Gb}{2\pi^2}\times \left[1+\beta-(1+\beta^2)^{1/2}-\beta\log(2\beta(1+\beta^2)^{1/2}-2\beta^2)\right] \tag{4}$$

and

$$\beta = \frac{\pi\delta'}{(1-\nu)}, \tag{5}$$

where δ' is the decrease in lattice misfit introduced by the interfacial dislocations. The critical diameter is obtained from (3) and (4):

$$d_{\mathrm{crit}} = \frac{b}{\delta^2}\frac{3(1-\nu)}{2\pi^2(1+\nu)}\times \left[1+\beta-(1+\beta^2)^{1/2}-\beta\log(2\beta(1+\beta^2)^{1/2}-2\beta^2)\right]. \tag{6}$$

Although the effect of temperature on the critical diameter was not included in the original analysis [40, 44], Røyset and Ryum [38] suggested the introduction of temperature dependency in (6) through the temperature dependencies of the Burgers vector of the Al matrix b and the lattice misfit δ. Note that the final expression does not depend explicitly on the shear modulus, the only elasticity parameter entering is the Poisson ratio of aluminum. The temperature dependence of the critical diameter is thus dominated by the lattice misfit originating from the differing thermal expansion parameters of the matrix and the precipitate, and complex inclusion of the elasticity parameters is avoided.

We have calculated the temperature dependence of critical diameter of Al_3X from the lattice misfit data obtained from the first principle methods in this study, using Eq. 6. For the Burgers vector we used b_{110} as in ref. [40], but included its temperature dependence based on our calculation of aluminum in the QHA. For the Poisson ratio ν we used the value obtained from a Voigt-Reuss-Hill average of our low temperature calculation of Al, which gave a value of $\nu = 0.30$. The temperature-dependent misfit δ was obtained as in Eq. 2, and as we are interested in the critical radius for coherency loss we took $\delta' \approx \delta$. The resulting critical radii for the $L1_2$ Al_3X precipitates considered here are plotted as a function of temperature in Fig. 5.

The critical diameters of Al_3Sc, Al_3Zr, Al_3Ti and Al_3Nb evolve differently with temperature, although again Al_3Sc and Al_3Zr are more similar, and Al_3Nb and Al_3Ti also show similarity. The temperature dependence of the critical diameter of Al_3Sc calculated here matches very well with the prediction in ref. [38]. Our results predict critical diameter ranges from 20 to 50 nm for Al_3Sc in the temperature range 300–700 K. This result is in good agreement with the observed coherency loss for Al_3Sc precipitates of 40 nm diameter [45]. At elevated temperatures up to 800 K the critical diameter increases and coherency is maintained up to 50 nm.

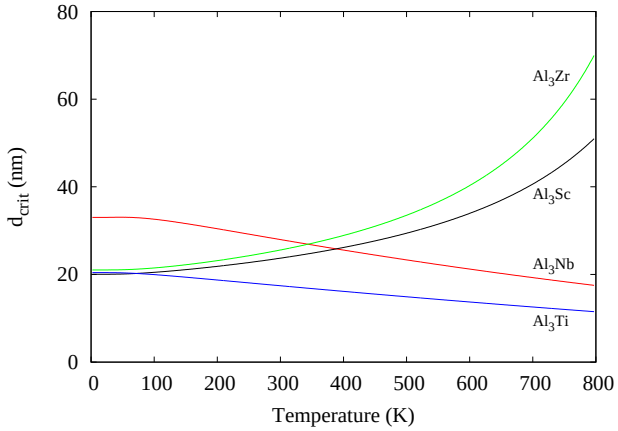

Figure 5: Comparison of critical diameters of $L1_2$ Al_3X (Al_3Nb red, Al_3Sc black, Al_3Ti blue, and Al_3Zr green, color on-line).

Al_3Zr precipitate shows a similar trend and is expected to remain coherent to a larger diameter. Our results predict that Al_3Zr remain coherent up to a diameter of about 70 nm for a temperature limit of 800 K. This is in reasonable agreement with the precipitates exhibiting coherency loss for a diameter of 70 nm [45]. At elevated temperature the critical diameter grows quickly and the precipitates remain coherent to a very large size. In contrast, Al_3Ti precipitates lose coherency beyond a small diameter of 20 nm and the critical diameter decreases with increasing temperature. Although adding Ti to a ternary Al_3(Sc,Ti) may decrease the lattice mismatch and remain coherent to a larger particle size, pure Al_3Ti loses coherency faster at elevated temperature. The Al_3Nb case is only marginally improved, with an initial critical diameter of about 35 nm followed by a decrease with increasing temperature.

The DO_{22} critical radii (data not shown) were determined for both the a and $c/2$ lengths, but because of the significant lattice mismatch at all temperatures (Fig. 4) the critical radii never exceed 4.5 nm. Clearly from this perspective the DO_{22} phases must be avoided in order to form strong, stable Al-Al_3X composites.

5. Conclusion

We have calculated the temperature-dependent critical diameter for coherency loss of Al_3Sc, Al_3Zr, Al_3Ti, and Al_3Nb in an Al_3X/α-Al heterophase system from the first principles. Our results agree with existing experimental observations at ambient temperature and extend the predictions at elevated temperatures. The critical radii of Al_3Sc and Al_3Zr both are about 20 nm at low temperature and show a strong increase with temperature. Al_3Nb and Al_3Ti on the other hand show critical radii that decrease with temperature. Furthermore, the DO_{22} phases of both Al_3Nb and Al_3Ti show much poorer lattice coherency and critical radii than do any of the $L1_2$ phases but are more stable energetically than the $L1_2$ phases. The trialuminides studied here can be considered as the end members of a ternary $L1_2$-Al_3(Sc,X) intermetallic systems, where X represents transition metals or rare Earth elements. Further studies are needed for $L1_2$-$Al_3(Sc_y,X_{1-y})$ intermetallic phases, with varying y to find intermetallics with improved coarsening resistance and a strong precipitation strengthening behavior.

Acknowledgment

We gratefully acknowledge financial support provided by Boeing Research and Technology (research contract 11-6392), and technical discussions and support provided by Boeing researchers Dr. Ryan Glamm and Dr. Stephen Gaydos. This research was enabled in part by support provided by WestGrid (www.westgrid.ca), ACEnet (www.ace-net.ca) and Compute Canada Calcul Canada (www.computecanada.ca).

References

[1] C. Hsu, C. Chang, P. Kao, N. Ho, C. Chang, Al-Al_3Ti nanocomposites produced *in situ* by friction stir processing, Acta Mater. 54 (19) (2006) 5241–5249.

[2] P. K. Mirchandani, R. C. Benn, K. A. Heck, Structure-Property Relationships in Elevated Temperature High Stiffness Mechanically Alloyed Al-Ti Based Alloys, in: Lightweight Alloys for Aerospace Applications, TMS, 1989.

[3] W. E. Frazier, M. J. Koczak, Grain Boundary and Orowan Strengthening of Elevated Temperature PM Aluminum-Titanium Alloys, in: Dispersion

Strengthened Aluminum Alloys, TMS, Warrendale, 1988.

[4] R. A. Varin, Intermetallic-reinforced light-metal matrix in-situ composites, Metall. Mater. Trans. A 33 (1) (2002) 193–201.

[5] J. Wu, S. Zheng, Z. Li, Thermal stability and its effects on the mechanical properties of rapidly solidified Al-Ti alloys, Mater. Sci. Eng. A 289 (1-2) (2000) 246–254.

[6] C. Rios, S. Milenkovic, P. Ferrandini, R. Caram, Directional solidification, microstructure and properties of the Al_3Nb–Nb_2Al eutectic, J. Cryst. Growth 275 (1) (2005) e153–e158.

[7] R. Boulechfar, S. Ghemid, FP-LAPW investigation of structural, electronic, and thermodynamic properties of Al_3V and Al_3Ti compounds, Phys. B (Amsterdam, Neth.) 405 (2010) 4045–4050.

[8] J. Røyset, N. Ryum, Scandium in aluminium alloys, Int. Mater. Rev. 50 (2005) 19–44.

[9] E. A. Marquis, D. N. Seidman, Nanostructural evolution of Al3Sc precipitates in an Al-Sc-Mg alloy by three-dimensional atom probe microscopy, Surf. Interface Anal. 36 (56) (2004) 559–563.

[10] S. Saha, J. Zwanziger, Elastic properties of ternary $(Al_x,Mg_{1-x})Sc$ random alloys from first principles methods, J. Alloy Compd. 610 (2014) 138–142.

[11] L. S. Kramer, W. T. Tack, M. T. Fernandes, Scandium in aluminum alloys, Adv. Mater. Processes 152 (4) (1997) 23.

[12] K. E. Knipling, R. A. Karnesky, C. P. Lee, D. C. Dunand, D. N. Seidman, Precipitation evolution in Al0.1Sc, Al0.1Zr and Al0.1Sc0.1Zr (at.%) alloys during isochronal aging, Acta Mater. 58 (15) (2010) 5184–5195.

[13] S. Das, L. Davis, High performance aerospace alloys via rapid solidification processing, Mater. Sci. Eng. 98.

[14] Y. Harada, D. Dunand, Creep properties of Al_3Sc and $Al_3(Sc,X)$ intermetallics, Acta Mater. 48 (13) (2000) 3477–3487.

[15] Y. Harada, D. Dunand, Microstructure of Al_3Sc with ternary transition-metal additions, Mater. Sci. Eng. A 329 (2002) 686–695.

[16] M. E. Drits, J. Dutkiewicz, L. S. Toropova, J.-. Salawa, The Effect of Solution Treatment on the Ageing Processes of Al-Sc Alloys, Cryst. Res. Technol. 19 (10) (1984) 1325 – 1330.

[17] E. Marquis, D. Seidman, M. Asta, C. Woodward, V. Ozoliņš, Mg Segregation at Al/Al3Sc Heterophase Interfaces on an Atomic Scale: Experiments and Computations, Phys. Rev. Lett. 91 (3) (2003) 18–21.

[18] G. Ghosh, S. Vaynman, M. Asta, M. Fine, Stability and elastic properties of L12-(Al,Cu)3(Ti,Zr) phases: Ab initio calculations and experiments, Intermetallics 15 (1) (2007) 44–54.

[19] X. Gonze, B. Amadon, P.-M. Anglade, J.-M. Beuken, F. Bottin, P. Boulanger, F. Bruneval, D. Caliste, R. Caracas, M. Cote, T. Deutsch, L. Genovese, P. Ghosez, M. Giantomassi, S. Goedecker, D. Hamann, P. Hermet, F. Jollet, G. Jomard, S. Leroux, M. Mancini, S. Mazevet, M. J. T. Oliveira, G. Onida, Y. Pouillon, T. Rangel, G.-M. Rignanese, D. Sangalli, R. Shaltaf, M. Torrent, M. Verstraete, G. Zerah, J. W. Zwanziger, Abinit: First-principles approach to material and nanosystem properties, Comput. Phys. Commun. 180 (2009) 2582–2615.

[20] X. Gonze, G. Rignanese, M. Verstraete, J. Beuken, Y. Pouillon, R. Caracas, F. Jollet, M. Torrent, G. Zerah, M. Mikami, P. Ghosez, M. Veithen, J. Raty, V. Olevano, F. Bruneval, L. Reining, R. Godby, G. Onida, D. R. Hamann, D. C. Allan, A brief introduction to the abinit software package, Zeit. Kristallogr. 220 (2005) 558–562.

[21] X. C. Gonze, First-principles responses of solids to atomic displacements and homogeneous electric fields: Implementation of a conjugate gradient algorithm, Phys. Rev. B 55 (1997) 10337–10354.

[22] X. C. Gonze, C. Lee, Dynamical matrices, born effective charges, dielectric permittivity tensors, and interatomic force constants from density-functional perturbation theory, Phys. Rev. B 55 (1997) 10355–10368.

[23] C. Lee, X. Gonze, Ab initio calculation of the thermodynamic properties and atomic temperature factors of sio_2 α-quartz and stishovite, Phys. Rev. B 51 (1995) 8610–8613.

[24] D. R. Hamann, Optimized norm-conserving Vanderbilt pseudopotentials, Phys. Rev. B 88 (2013) 085117.

[25] J. P. Perdew, K. Burke, M. Ernzerhof, Generalized gradient approximation made simple, Phys. Rev. Lett. 77 (1996) 3865–3868.

[26] N. Marzari, D. Vanderbilt, A. De Vita, M. Payne, Thermal contraction and disordering of the al (110) surface, Phys. Rev. Lett. 82 (16) (1999) 3296.

[27] A. S. Cooper, Precise lattice constants of germanium, aluminum, gallium arsenide, uranium, sulphur, quartz and sapphire, Acta Crystallogr. 15 (6) (1962) 578–582.

[28] G. Brauer, Über die kristallstruktur von $TiAl_3$, $NbAl_3$, $TaAl_3$, und $ZrAl_3$, Z. Anorg. Allg. Chem. 242 (1939) 1–22.

[29] J. F. Cannon, H. T. Hall, Effect of high pressure on the crystal structures of lanthanide trialuminides, J. Less-common Met. 40 (3) (1975) 313–328.

[30] S. Srinivasan, P. Desch, R. Schwarz, Metastable phases in the Al_3X (X = Ti, Zr, and Hf) intermetallic system, Scr. Metall. Mater. 25 (11) (1991) 2513–2516.

[31] P. Norby, A. N. Christensen, Preparation and structure of Al_3Ti, Acta Chem. Scand., Ser. A 40 (1986) 157–159.

[32] A. Wilson, The thermal expansion of aluminium from 0 to 650°c, Proc. Phys. Soc., London 53 (3) (1941) 235.

[33] F. Nix, D. MacNair, The thermal expansion of pure metals: copper, gold, aluminum, nickel, and iron, Phys. Rev. 60 (8) (1941) 597.

[34] M. Asta, V. Ozoliņš, Structural, vibrational, and thermodynamic properties of al-sc alloys and intermetallic compounds, Phys. Rev. B 64 (9) (2001) 094104.

[35] Y. Harada, D. Dunand, Thermal expansion of Al_3Sc and $Al_3(Sc_{0.75}X_{0.25}$, Scr. Mater. 48 (3) (2003) 219–222.

[36] C.-P. Reip, G. Sauthoff, Deformation behaviour of the intermetallic phase Al_3Nb with DO_{22} structure and of Al_3Nb-base alloys: Part I. physical properties and short-term behaviour, Intermetallics 1 (1993) 159–169.

[37] R. Boulechfar, S. Ghemid, H. Meradji, B. Bouhafs, FP-LAPW investigation of structural, electronic, and thermodynamic properties of Al_3V and Al_3Ti compounds, Phys. B (Amsterdam, Neth.) 405 (2010) 4045–4050.

[38] J. Røyset, N. Ryum, Some comments on the misfit and coherency loss of Al_3Sc particles in Al–Sc alloys, Scr. Mater. 52 (2005) 1275–1279.

[39] Y. Harada, D. Dunand, Microstructure of Al_3Sc with ternary rare-earth additions, Intermetallics 17 (2009) 17–24.

[40] S. Iwamura, Y. Miura, Loss in coherency and coarsening behavior of Al_3Sc precipitates, Acta Mater. 52 (3) (2004) 591–600.

[41] M. Y. Drits, L. Ber, Y. G. Bykov, L. Toropova, G. Anastas'eva, Ageing of alloy al-0 multiplied by 3 at.% sc., Phys. Met. Metallogr. (Transl. of Fiz. Met. Metalloved.) 57 (6) (1984) 118–125.

[42] W. C. Johnson, P. Voorhees, Elastic interaction and stability of misfitting cuboidal inhomogeneities, J. Appl. Phys. 61 (1987) 1610–1619.

[43] M. McCormack, A. Khachaturyan, J. Morris Jr, A two-dimensional analysis of the evolution of coherent precipitates in elastic media, Acta Metall. Mater. 40 (2) (1992) 325–336.

[44] W. Jesser, On the theory of loss of coherency by spherical precipitates, Philos. Mag. 19 (161) (1969) 993–999.

[45] K. E. Knipling, D. C. Dunand, D. N. Seidman, Precipitation evolution in Al–Zr and Al–Zr–Ti alloys during aging at 450–600 c, Acta Mater. 56 (2008) 1182–1195.